A Hybrid Single-Mode Laser Based on Slotted Silicon Waveguides

Mengke Li, Lianxue Zhang, Hongyan Yu, Lijun Yuan, Qiang Kan, Weixi Chen, Ying Ding, Shiyan Li, Junping Mi, Guangzhao Ran and Jiaoqing Pan*

***Abstract*—An InGaAsP-Si hybrid single-mode laser based on etched slots in silicon waveguides was demonstrated operating at 1543 nm. The InGaAsP gain structure was bonded onto a patterned silicon-on-insulator (SOI) wafer by selective area metal bonding (SAMB) method. The mode-selection mechanism based on a slotted silicon waveguide was applied in which the parameters were designed using the simulation tool "Cavity Modeling Framework" (CAMFR). The III-V lasers employed buried ridge stripe (BRS) structure. The whole fabrication process only needs standard photolithography and inductively coupled plasma (ICP) etching technology, which reduces cost for ease in technology transfer. At room temperature, a single mode of 1543 nm wavelength at a threshold current of 21 mA with a maximum output power of 1.9 mW in continuous-wave regime was obtained. The side mode suppression ratio (SMSR) was larger than 35 dB. The simplicity and flexibility of the fabrication process and a low cost make the slotted hybrid laser a promising light source.**

***Index Terms*—Hybrid silicon laser, slots, CAMFR, single-mode laser, buried ridge stripe (BRS) structure, selective area metal bonding (SAMB) method**

I. Introduction

In recent years silicon photonics as an integration platform has been a focus of optoelectronics research because of promise of low-cost, high-volume, manufacturing in silicon allowing for economical optical interconnects in applications [1]-[2]. Optical interconnects to and on silicon-on-insulator (SOI) substrates are now being considered as a promising candidate to overcome the limitations of electrical interconnects [3]. However, the fabrication of an efficient laser on the silicon platform is still challenging due to silicon's indirect bandgap. Among the several types of III-V/Si hybrid lasers [4]-[5], bonding is one of the most effective and practical ways to realize silicon hybrid lasers, where the optical mode of an III-V laser evanescently couples to a silicon waveguide. Quite a few of bonding methods have been used to develop silicon evanescent lasers, such as direct wafer bonding [6]-[8], benzocyclobutene (BCB) bonding [9]-[10], and selective area metal bonding (SAMB) [11]-[12]. Of these bonding methods, the SAMB method shares the following advantages of other bonding methods: low thermal stress, no critical cleanness requirement, good thermal conductivity and electrical performance [12]. In this letter, we choose the SAMB method to realize the hybrid InGaAsP-Si evanescent laser, which laterally separates the optical coupling area and the metal bonding area to avoid strong light absorption of metal in the optical coupling area.

For achieving single-mode silicon hybrid lasers, distributed feedback (DFB) or distributed Bragg reflection (DBR) resonators have been bonded on the SOI platform [13]. In addition, etching distributed feedback gratings on the SOI platform by holographic lithography and based on SAMB bonding technology can also achieve single-mode lasing [14]. However, fabrication of these devices generally needs expensive, time-consuming manufacturing techniques such as electron-beam (e-beam) lithography and focused ion beam for patterning, which is quite expensive compared with the standard photolithography, and often requires complex regrow steps. For avoiding the complex regrowth, high-resolution processes and expensive e-beam lithography, a single-mode laser has been presented, which relied on slots along the cavity in a Fabry-Perot (FP) laser, and slots within the cavity result in effective index perturbations that introduce a modulation and improve the spectral purity of FP lasers. The slotted lasers have been demonstrated with very good characteristics [15]-[16]. Based on it, slotted feedback single-mode hybrid lasers have been demonstrated [17]-[18]. By etching optimized slots on silicon waveguides, researchers have achieved single-mode hybrid lasers by a direct bonding method. The main advantage of this technique is that it minimizes the fabrication complexity thereby increases reliability while reducing cost. In this letter, we combine the SAMB bonding method and slotted waveguides to demonstrate a single-wavelength hybrid III-V/Si laser for the first time. Compared with previous work [19], the p-InP substrate flip-chip bonding method is a thick-film bonding method, which can greatly improve the bonding yield.

This work was supported by the National 863 Project (Grant No.2012AA012203), and the National 973 Program (Grant No.2013CB632105)

Mengke Li, Hongyan Yu, Lijun Yuan, Qiang Kan, Shiyan Li, Junping Mi and Jiaoqing Pan are with Key Laboratory of Semiconductor Materials Science, Institute of Semiconductors, Chinese Academy of Science, Beijing 100083, China.(E-mails:limengke11@semi.ac.cn; hyyu09@semi.ac.cn; ljyuan@semi.ac.cn; kanqiang@semi.ac.cn; lishiyan@semi.ac.cn; mijunping11@semi.ac.cn; jqpan@semi.ac.cn;)

Lianxue Zhang, Weixi Chen, Guangzhao Ran are with State Key Lab for Macroscopic Physics and School of Physics, Peking University, Beijing 100871,China.(E-mails:zlxxfzm@163.com; wxchen@pku.edu.cn; rangz@pku.edu.cn;)

Ying Ding is with Electronic and Nanoscale Engineering, School of Engineering, University of Glasgow, G12 8LT, Glasgow UK. (E-mail: ying.ding@glasgow.ac.uk ;)

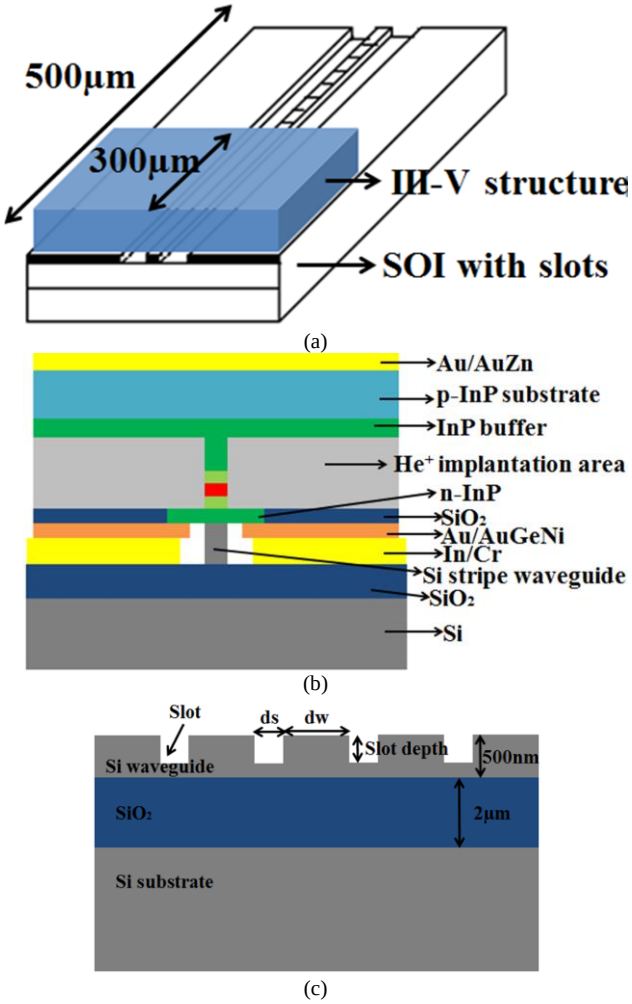

Fig. 1. (a) 3-D schematic structure of the hybrid laser. (b) The transverse cross-section of the slotted hybrid laser. (c) Simplified 2-D structure with the slots on silicon waveguide in simulation.

These slot parameters were calculated by the simulation tool CAMFR [20] and fabricated through standard low-cost semiconductor processes. Finally we obtain a 21 mA threshold current with a maximum output of 1.9 mW in continuous-wave regime at room temperature. The side-mode suppression ratio (SMSR) is larger than 35 dB from experiments.

II. Device Structure and Simulations

The three-dimensional (3-D) schematic structure and the transverse cross-section of the slotted InGaAsP-Si hybrid laser are shown in Figs. 1(a) and 1(b). A buried ridge stripe (BRS) InGaAsP structure is flip-chip bonded onto a pattern SOI wafer with SAMB method and etched slots are outside the III-V structure. The III-V laser has the same epitaxial structure as in [13]. The SOI substrate has a 500nm-thick top silicon layer and a 2 μm-thick SiO_2 layer. The strip waveguide is formed on the top silicon layer with a width of 3 μm. In this structure, one side of the Si waveguide has multiple uniformly distributed slots,

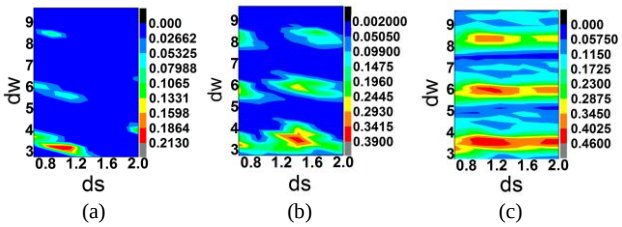

Fig. 2. Contour plots of the simulated amplitude reflection versus slot width d_s (micron) and spacing d_w (micron) with the slot depths of (a) 100 nm, (b) 200 nm, (c) 300 nm.

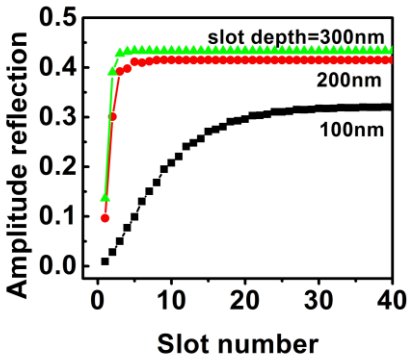

Fig. 3. Calculated amplitude reflection from a group of slots versus the slot number with the slot depths of 100 nm, 200 nm, and 300 nm, respectively.

which act as a high-order surface DBR and a single mode is specifically selected. So in simulations, we only consider the SOI part.

The slot parameters on SOI waveguides such as the slot width d_s, the spacing d_w, the slot depth, and the slot number are key parameters that influence the hybrid laser single-mode performance and have to be optimized in the design. We use the simulation tool CAMFR to calculate and optimize these slot parameters. The simplified two-dimensional (2-D) structure on SOI substrates in the simulation is shown in Fig. 1(c). In the simulation, the index of refraction of Si and SiO_2 are 3.47 and 1.47, respectively. The Bragg wavelength was always set to be 1550 nm.

The contour plots of the calculated amplitude reflection are given in Fig. 2, which show that the slot width d_s and spacing d_w influence the reflection strongly at different slot depths of 100 nm, 200 nm and 300 nm. In the simulation we set the slot number to be a fixed value of 100. The slot width of around 1 μm was the focus, so the slots can be fabricated by standard photolithography. There exists high reflection peaks with slot widths of around 1.1 μm. Therefore, we obtain the optimized slot width and spacing at every slot depth with the maximized reflection as the optimizing parameters.

Based on the simulation results above, the amplitude reflection versus the slot number was calculated at every slot depth as shown in Fig. 3. In the simulation, the slot width and spacing from Fig. 2 were used. In Fig. 3, with the increase of the slot number, the amplitude reflection increases until it gradually saturates. In this case, for the trade-off between maximizing the reflectivity and minimizing the size of whole

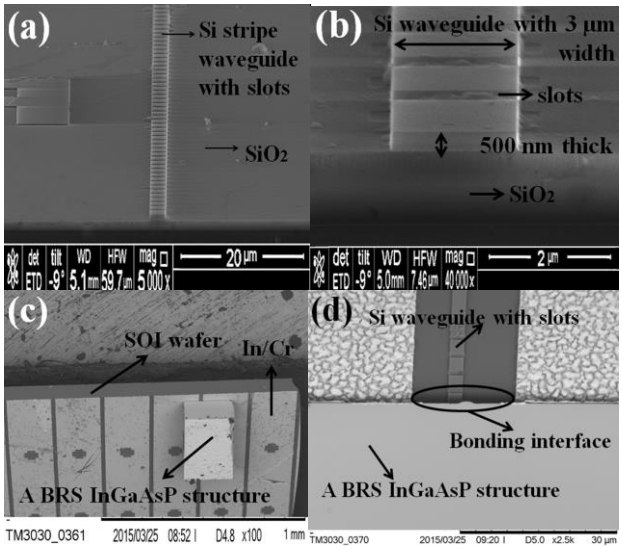

Fig. 4. (a) and (b) SEM images of SOI with slots. (c) and (d) SEM images of III-V wafer bonded onto an SOI strip waveguide with slots.

device, the slot number should be small. So the slot depth of 300 nm was chosen as the optimized parameter with the slot number of about 25. The reflection spectrum has narrow bandwidth of about 2.1 nm according to our calculation. This helps achieve a good mode operation with the minimum threshold. This suggests that the total length of the slotted region of the SOI waveguide is 185 μm, which keeps the slotted region of the SOI waveguide outside the bonded III-V structure with the 300 μm-length single chip.

From the simulation results above, the optimized slot width and spacing of 1.1 μm and 6.3 μm were obtained, respectively. The slot number is 25 at the slot depth of 300 nm. Based on the simulation results, the slotted hybrid laser was fabricated with the optimized slot parameters and measured the device characteristics as follows.

III. Fabrication

The III-V wafer structure was grown on a p-InP substrate by two-step metal organic chemical vapor deposition (MOCVD). In the first growth step, a p-InP buffer and an i-InP layer were grown on the substrate. The active layer consists of InGaAsP multi-quantum wells (MQWs) active region, which is bounded by the separate confinement hetero-structure (SCH) layer. Then a 3 μm wide ridge down to the p-InP layer was achieved by photolithography and wet chemical etching in bromine solution. In the second MOCVD growth, a 500 nm thick n-InP cladding layer was grown on this ridge stripe structure as the current injection layer. Then, He^+ implantation was carried out for the n-InP layer to create highly resistive regions on both sides of the buried ridge stripe. After that, a 300 nm thick and 20 μm wide window SiO_2 layer was deposited for further improving current confinement. After depositing a 300nm-thick AuGeNi/Au contact on the surface, a 4 μm width optical coupling window was opened with the buried ridge stripe in the center. Then, an AuZn layer was thermally evaporated on the back side after the p-InP substrate thinning. Finally, the wafer was annealed at 420 ℃ for 35 s to form a good ohmic contact.

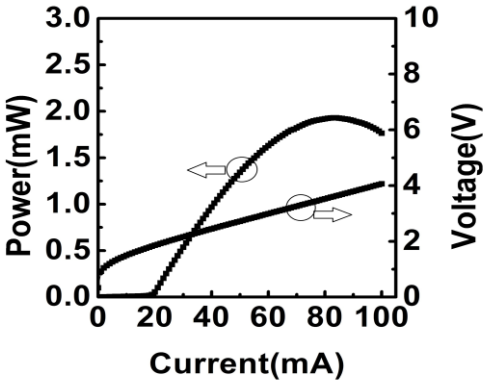

Fig. 5. Measured light-current (L-I) and current-voltage (I-V) curves under the continuous-wave regime at room temperature.

In the SOI region, two steps of ICP etching were used to form the slots and the ridge, shown in Figs. 4(a) and 4(b). For the first fabrication run photolithography was used to pattern the slots and ICP dry etching with Cl_2/N_2 gas combinations were used to form the slots. Afterwards a 500nm-height and 3 μm-width ridge was determined by the dry etching process. Metal lift-off technology was adopted to selectively deposit the bonding metal on each side of the silicon waveguide. A 200nm-thick In/Cr was used as the bonding metal. This is widely used in metal bonding due to its good electrical and thermal conductivity. Finally the SOI wafer was thinned to about 100 μm thick in order to be diced into bars easily and to retain good emitting surfaces.

Finally, the III-V wafer was cleaved to single chips of length 300 μm and flip-chip bonded to the SOI wafer by a FINETECH Lamda A6 bonder with an alignment accuracy of ±0.5 μm. The bonding process was done at 170 ℃ for 5 min under a pressure of about 2.3 MPa in N_2 atmosphere. A scanning-electron micrograph (SEM) image of the final fabricated hybrid laser is shown in Figs. 4(c) and 4(d).

IV. Experimental Results

The output power of the hybrid laser was measured from one facet of the device using a large-area photo-detector positioned in close proximity to the facet, to ensure maximum power output detection. Fig. 5 shows the measured light-current (L-I) and current-voltage (I-V) curves for the fabricated laser under continuous-wave regime at room temperature, which exhibits a threshold current (I_{th}) of about 21 mA corresponding to a threshold current density (J_{th}) of 2.325 kA/cm^2. Considering two facets of the laser, the maximum output power is about 1.9 mW with a slope efficiency of about 0.023 mW/mA at an injection current of 80 mA. The series resistance of the hybrid laser is 16.5 Ω. This is because the SOI wafer was thinned and diced into bars. From Fig. 5, the slope efficiency is not high and this is mainly because the high slot losses result in scattering losses and affect the performance. Besides, the imperfect shape

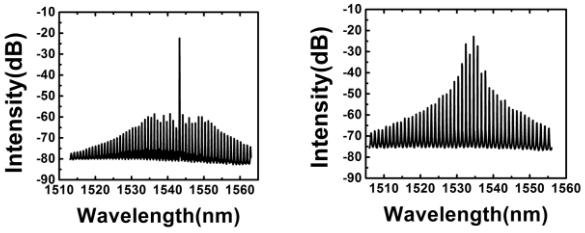

(a) (b)

Fig. 6. (a) The optical spectrum of the slotted hybrid laser at the continuous injection current of 60 mA at room temperature. (b) The lasing spectrum of un-slotted hybrid laser at the same test condition.

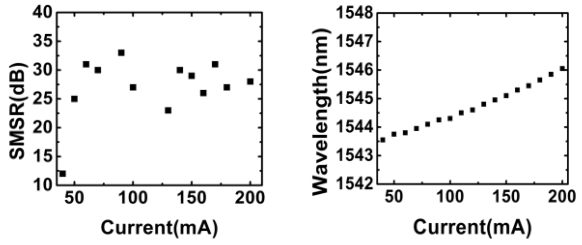

(a) (b)

Fig. 7. Drive current dependence of (a) SMSR and (b) wavelength.

of the slots also influences the reflection. Further experiments with optimized parameters are in progress.

The optical spectrum of the slotted hybrid laser was then measured and shown in Fig. 6(a). The output power was collected by a lensed multimode fiber placed near the silicon waveguide connected to an optical spectrum analyzer. From Fig. 6(a), it can be observed that a single longitudinal mode lasing spectrum of the silicon evanescent laser is presented at continuous injection current of 60 mA. The laser diode has a lasing peak of 1543 nm and the SMSR is approximately 37 dB. For comparison, the spectrum of the hybrid laser without slots was measured at the same test conditions, shown in Fig. 6(b). It is obvious that for the un-slotted hybrid laser it is a typical FP spectrum with many longitudinal modes. Comparing the two spectra, we observe that the spectrum of the hybrid laser can be modified by etching slots at a chosen spacing, width and depth in the SOI strip waveguide. As the injection current increases, the laser maintains single-mode operation as in Fig. 6(a), which demonstrates that the slots improve the wavelength stability of the single mode. Moreover, as the current increases, the dominant mode with the SMSR is around 30 dB as shown in Fig. 7(a). The drive current dependence of the prominent modes is shown in Fig. 7(b), which demonstrates the wavelength shift with a current is ~0.02 nm/mA.

V. Conclusion

In summary, we have designed and fabricated a single-mode evanescent hybrid laser with SAMB bonding method based on etching slots on the SOI platform. From the optimized slot parameters modeled by CAMFR, we obtain a threshold current of 21 mA with a maximum output power of 1.9 mW in the continuous-wave regime at room temperature. The results show that etching slots can provide a mode-selection mechanism. Only photolithography and ICP etching technology were used for the fabrication of the silicon waveguides. SMSR of around 37 dB was obtained in experiments. The simplicity and flexibility of the fabrication process and a low process make the slotted hybrid laser a promising light source.

References

[1] D. Liang and J. E. Bowers, "Recent Progress in Lasers on Silicon," *Nat. Photonics*, vol.4, pp.511-517, 2010.
[2] T. Wang, et al., "1.3-μm InAs/GaAs Quantum-Dot Lasers Monolithically Grown on Si Substrates," *Opt. Express*, vol.19, pp.11381-11386, 2011.
[3] Alexander W. Fang and Hyundai Park, "Hybrid Silicon Evanescent Devices," *Materials Today*, vol.10, pp.28-35, July-Aug. 2007.
[4] H. Rong et al., "A Continuous-Wave Raman Silicon Laser," *Nature*, vol.433, no.725, 2005.
[5] Boyraz, et al., "Demonstration of a Silicon Raman Laser," *Opt. Express*, vol.12, pp.5269, 2004.
[6] A. W. Fang, et al., "Electrically Pumped Hybrid AlGaInAs-Silicon Evanescent Laser," *Opt. Express*, vol.14, pp. 9203-9210, 2006.
[7] H. Chang, et al., "1310 nm Silicon Evanescent Laser," *Opt. Express*, vol.16, pp.11466-11471, 2007.
[8] A. W. Fang, et al., "Integrated AlGaInAs Silicon Evanescent Racetrack Laser and Photodetector," *Opt. Express*, vol.15, pp.2315-2322, 2007.
[9] S. Stankovic, et al., "1310-nm Hybrid III-V/Si Fabry-Perot Laser Based on Adhesive Bonding," *IEEE Photon. Technol. Lett.*, vol.23, pp.1781-1783, 2011.
[10] S. Stankovic, et al., "Hybrid III-V/Si Distributed-Feedback Laser Based on Adhesive Bonding," *IEEE Photon. Technol. Lett.*, vol.24, pp.2155-2158, 2012.
[11] T. Hong, et al., "Bonding InGaAsP/ITO/Si Hybrid Laser with ITO as Cathode and Light-Coupling Material," *IEEE Photon. Technol. Lett.*, vol.24, pp.712-714, 2012.
[12] L. J. Yuan, et al., "A Buried Ridge Stripe Structure InGaAsP-Si Hybrid Laser," *IEEE Photon. Technol. Lett.*, vol.27, pp.352-355, 2015.
[13] CHEN Ting, et al., "Electrically Pumped Room-Temperature Pulsed InGaAsP-Si Hybrid Lasers Based on Metal Bonding." *CHIN. PHYS. LETT.*, vol.26, no.6, pp.064211, 2009.
[14] Li Tao, et al., "4-λ InGaAsP-Si Distributed Feedback Evanescent Lasers with Varying Silicon Waveguide Width," *Optics Express*, vol.22, pp.5448-5454, 2014.
[15] Q. Y. Lu, W. H. Guo, D. Byrne, and J. F. Donegan, "Design of Slotted Single-Mode Lasers Suitable for Photonic Integration," *IEEE Photon .Technol. Lett.*, vol.22, no.11, pp.787–789, Jun.1, 2010.
[16] W. H. Guo, *et al.*, "Integrable Slotted Single-Mode Lasers," *IEEE Photon. Technol. Lett.*, vol.24, no.8, pp.634–636, Apr.15, 2012.
[17] Yejin Zhang, et al., "Slotted Hybrid III-V/Silicon Single-Mode Lasers," *IEEE Photon Technol. Lett.*, vol.25, no.7, Apr.1, 2013
[18] Yejin Zhang, et al., "A III-V/Silicon Hybrid Racetrack Ring Single-Mode Laser with Periodic Microstructures," *Optics Communications*, pp.301-302, 2013.
[19] T. Hong, et al., "A Selective-Area Metal Bonding InGaAsP-Si Laser," *IEEE Photon. Technol. Lett.*, vol.22, pp.1141-1143, 2010.
[20] CAMFR—CAvity Modeling FRamework, P. Bienstman, L. Vanholme, M. Ibanescu, P. Dumon, and R. Baets. [Online]. Available: http://camfr.sourceforge.net/